PHYSICAL LIMITS TO THE PERFORMANCE OF IMAGING SYSTEMS

A half-century of electronic imaging technology has begun to match and even surpass the performance of the eye, an amazingly sophisticated photon detector perfected by evolution.

Albert Rose and Paul K. Weimer

Our visual system provides our principal contact with the world around us. This system, thanks to millions of years of natural development, achieved a high degree of perfection long before humans arrived on the scene. To attain such perfection, these evolutionary processes had to recognize the quantum nature of light—a remarkable accomplishment.

A wide variety of electronic surrogates for the human eye have been developed in the last half century. In this short time they have succeeded in matching, and in some cases exceeding, the performance of the eye. In essence, the performance of the eye and of the electronic imaging systems is measured by their ability to count the incident photons. The meaning of this counting process, and the variety of ways of achieving it in both the human and electronic systems, is the subject of this article.

The human eye

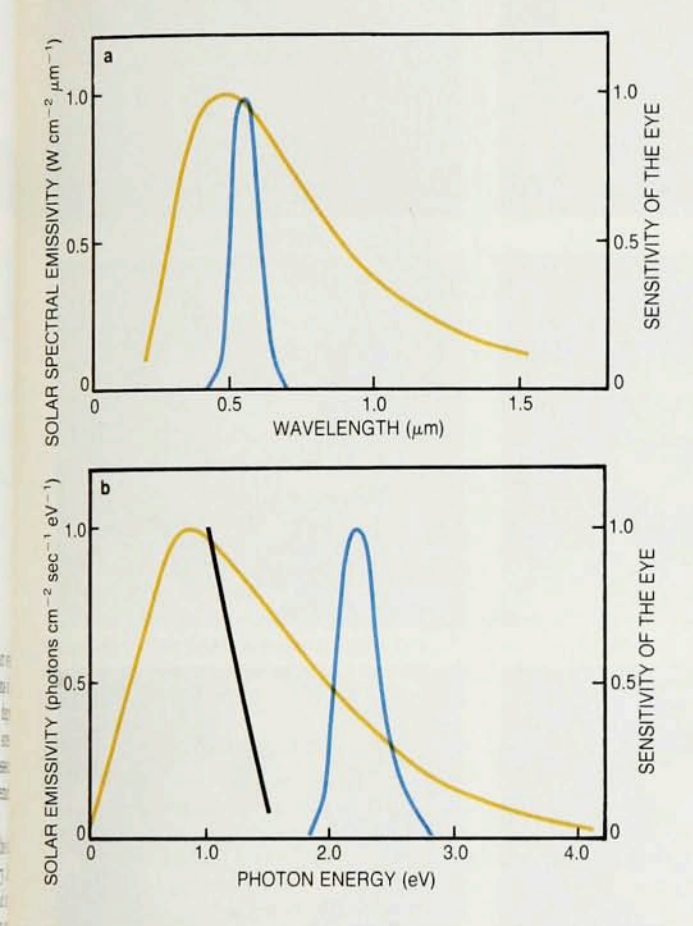
The human eye is a nearly perfect imaging system. As such it can serve as a portable, readily accessible and remarkably sophisticated model of what is meant by a

nearly perfect imaging system.

It is true, on the one hand, that the nervous system and the mind are considerably more sophisticated than the eye. On the other hand, we have no models of the perfect nervous system or the perfect mind against which we can measure the accomplishment of nature. In the case of the eye, we can easily and quantitatively define the perfect parameters and compare them with our actual eyes. A perfect eye should be able to count incoming photons; its resolution should be limited only by diffraction; and the amplification of the retina should be sufficient to increase the energy of a single photon to the energy of a nerve pulse.

Other properties of the eye should be matched to the needs of the human system. For example, the "exposure time" of the eye should be matched to the response time of the human body. (The exposure, or "storage," time of the eye or any other imaging system is the effective time over which it integrates the the light input to produce an

Albert Rose is a consultant and a visiting scientist at the Chronar Corporation, Princeton, New Jersey. Paul K. Weimer is a consultant and former Fellow of the Technical Staff at the RCA David Sarnoff Research Center in Princeton



Solar spectrum at the top of the atmosphere (yellow curves) compared with the standard sensitivity curve of the eye at ordinary light levels (blue curves). When both are plotted against wavelength (a) and the solar spectrum is given in watts per unit area per unit wavelength, their peaks nearly coincide. When they are plotted against photon energy (b) and the solar spectrum is given as the photon flux per unit energy, its peak shifts to well below the eye's sensitivity maximum. This keeps us from being bothered at night by thermal excitations in the retina. The photon flux of the night sky is shown by the black curve. (The curves are normalized to unity at their maxima.) Figure 1

output signal.) Also, extraneous sources of optical noise, such as thermal excitations, should be excluded.

The essential properties of the human eye are common to most vertebrates. Its spectral response extends over the wavelength range from 400 to 700 nanometers. The photosensitive material is rhodopsin.

This spectral response is an excellent example of the near-perfect design of the eye. It had to exclude interference by thermal excitations. In doing so, it had to recognize implicitly the quantum nature of light. This problem was already solved for the deep-sea fish over a hundred million years ago—some time before Planck won the Nobel Prize for explicitly discovering the quantum nature of light.

Solar spectrum

The spectral response of the human eye peaks at about 500 nm. It is widely, and quite naturally, thought that this peaking coincides closely with the peak of the solar spectrum. If one plots the solar spectrum, as is commonly done, in terms of watts per cm² per micron versus wavelength, the solar spectrum does indeed peak at 550 nm, as shown by the yellow curve in figure 1a. But the eye is a photon counter and not a light-intensity meter. The solar spectrum should therefore be plotted in terms of photons per cm² per second per eV versus the photon energy hv. When this is done, as in figure 1b, the solar spectrum peaks at a wavelength of about a thousand nanometers in the near infrared rather than at the 550-

nm sensitivity peak (blue curve) of the eye. In terms of photon energies, 1-eV photons are the most abundant in solar radiation, but the eye is most efficient at counting 2.2-eV photons.

One might think that this is one of nature's mistakes. But in fact, if nature had designed the eye to peak at 1 eV, where the solar radiation peaks, we would be deprived of our night vision. Our visual field would be flooded by "fireflies"—thermally excited optical excitations of the retina. It was to avoid these thermal excitations, indicated in the black curve in figure 1b, that nature carefully shifted our visual sensitivity peak from 1 eV to about 2.2 eV so that we can ignore these thermal excitations with minimum loss of visible solar photons.

An excellent update of the photochemical properties of the human eye is presented in a recent paper by Julie L. Schnapf and Denis A. Baylor. They cite experimental evidence that a single retinal element (a rod cell) can record individual photons. This implies that the rod can amplify the energy of a single photon to the energy of a nerve pulse—a millionfold gain. This high gain is achieved photochemically. Each photon opens up a channel in the membrane of a rod cell through which a million sodium ions are then allowed to pass. This occurs at very low light levels near the absolute threshold of the eye, at scene illuminations of about 10^{-7} foot-candles. As the scene illumination is increased by a factor of 10^{10} , to the level of bright sunlight, the gain factor is steadily reduced by a factor of about 10^3 . If now the observer



Testing the quantum efficiency of the eye. These electronic images of the same subject were made with the number of photons indicated. The corresponding brightness labels (in foot-lamberts) are calculated as if the imaging system has 10% quantum efficiency. If then the subject, when illuminated with a given brightness, looks to the eye like the electronic image with the same brightness label, we conclude that the quantum efficiency of the eye is 10%. Figure 2

moves from bright sunlight into an ambiance of moonlight $(10^{-2} \,$ foot-candles) or starlight $(10^{-5} \,$ foot-candles), the observer requires some minutes to adapt to the darkness and regain the millionfold amplification characteristic of human night vision.

Quantum efficiency of the eye

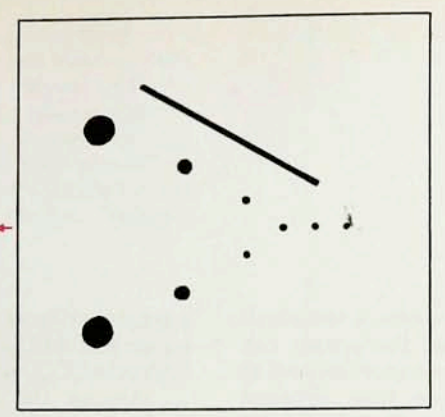
In the 1940s this process of dark adaptation was misinterpreted as an increase in sensitivity (quantum efficiency) by a factor of a thousand. Actually, the sensitivity of the eye is almost constant over an enormous range in light intensity. If one assumes that exposure time is independent of light intensity, the sensitivity of the eye appears to drop by a factor of about 3 in going from starlight to sunlight.³ Schnapf and Baylor, however, cite evidence that exposure time is reduced by about the same factor of 3 between starlight and sunlight. Taking this reduction of effective exposure time into account leads to the conclusion that the quantum efficiency of the eye is nearly constant from starlight to sunlight. Coupled with the eye's automatic gain control and its avoidance of thermal excitations, this is a triumph of

sophisticated design engineered by nature.

Measurements of the actual overall quantum efficiency of the eye³ lead to values of about 10%. Considering the near perfection of the other parameters of the eye, this relatively low efficiency comes as something of a surprise. A good part of the lowered efficiency can be ascribed to the fact that the retina of the eye does not absorb 100% of the incident photons. Why the absorption is so low is not at all clear. That it is low even in nocturnal mammals is demonstrated by the yellow appearance of cats' eyes illuminated at night. The yellow is due to light passing through the retina and then being reflected back out again by a yellow membrane behind the retina called the tapetum. The reason for this double passage is not clear. In the human eye this membrane is black. The retina of a salamander has large empty spaces between the rods.²

A second consideration that should contribute as much as a factor of 2 reduction in sensitivity is the switch from monochrome vision in low light to color vision in bright light. Color vision is mediated by a collection of retinal cells called cones. Approximately a third of the cones are red sensitive, a third are green sensitive, and a







Photon randomness limits perception at low illumination. The test pattern of bar and disks at center is subtracted from the randomly uniform photon distribution at left to yield the imperfectly discerned pattern at right. One must remove about 25 photon dots before a black disk is discernible. The diagonal bar is easier to see. The red arrows point to a false disk image due to random local depletion. **Figure 3**

third are blue sensitive. Roughly half the cones respond to any given wavelength because the color response curves of the three varieties of cones overlap considerably. The switch from color to monochrome vision is clearly an attempt to gain additional sensitivity in low light. At nightfall the antelope is more interested in the tiger's shape than in its color.

The human eye can serve our discussion of imaging technology as a convenient example of a nearly perfect imaging system—perfected for us by millions of years of evolutionary fine tuning.

Information from photons

How do we know that the eye is so close to ideal perfection? The answer is quite simple. Using electronic imaging systems developed for television, we can produce a series of pictures generated by various known numbers of photons, as shown in figure 2. We can then focus the same number of photons on our own eyes. If what we see matches the electronically generated pictures, we can conclude that our eyes are operating with a quantum efficiency of 100%. But if we need ten times as many photons to obtain a visual picture matching the electronically generated picture, we must conclude that the efficiency of our visual system is only 10%. We label the pictures in figure 2 with brightness levels calculated as if the imaging system recording them had an efficiency of 10%. Then we need only look at the same test subject at a given of scene brightness and see if our visual image matches the corresponding picture. If the answer is ves, the efficiency of our visual system is 10%. This is, in fact, the basis for our estimate of the quantum efficiency of the eye.

We can make use of the more rigorous test pattern in the center of figure 3. The number of photons N required to see a disk of diameter D against a background of area Aand contrast C is given by⁴

$$N = \frac{Ak^2}{D^2C^2E} \tag{1}$$

if the overall quantum efficiency is E. The contrast is defined as the fractional difference between the brightness of the disk and its background. Figure 3 clarifies the role of the parameter k, the threshold signal-to-noise ratio.

The left panel of figure 3 is a photograph of a random distribution of photons recorded at a low level of "uniform" illumination. At the right is the same photon distribution minus all the photons screened out by the test pattern in the central panel. How many photons

must we remove from a local region to make the removal visible? If that number is n, then the signal is n, the noise due to the randomness of the photons is $n^{1/2}$ and the signal-to-noise ratio is $n^{1/2}$. The removal of a single photon is obviously not detectable. In figure 3 one has to remove about 25 photons to render a denuded disk clearly visible. Therefore the threshold signal-to-noise ratio k in this case is roughly 5.

The small red arrows in figure 3 indicate a *false* image of a black disk due to the randomness of the photon distribution. Note also that the long diagonal bar in the test pattern is clearly visible even though it is thinner than the smallest black disks in the pattern. This shows that bar-shaped test patterns, commonly used to measure the resolution of photographic film, grossly overestimate the film resolution relative to disk patterns. The bar is visible because the eye integrates over the entire length of the bar.

In an ideal system the only noise source is the random nature of the photons. A nonideal system in which the dominant noise comes from the first stage of the amplifier would show a decreased visibility of the pattern of disks. Also, the presence of optical defects such as aberrations in the lens would tend to render the smaller disks invisible. For nocturnal mammals, however, photon randomness is a more severe limiting factor than lens aberration. That's why the lemur, for example, comes out ahead with a pupil that opens to a diameter equal to its focal length-a maximum aperture of f/1. (The largest aperture of the human eye is f/2.) In spite of the bad spherical aberration that must characterize a lens aperture as large as f/1, the paucity of photons in starlight probably limits the resolution of the lemur's visual field to disks too large to be significantly affected by these aberrations.

To test the resolving power of an imaging system, one should employ test patterns with black disks of varying diameter and contrast. Using a number of such patterns with different background photon densities, we find³ that equation 1 provides a very satisfactory prescription for how many photons it takes to discern a simple feature.

Physical limits of electronic sensing

The function of an electronic image sensor is to generate electrical signals that describe accurately the optical images focused on its array of photosensitive picture elements (pixels). Unlike the eye, whose photoreceptors are connected in parallel to the brain through a million channels, the array of sensor pixels is sampled in rapid sequence to produce a single, time-varying output signal.

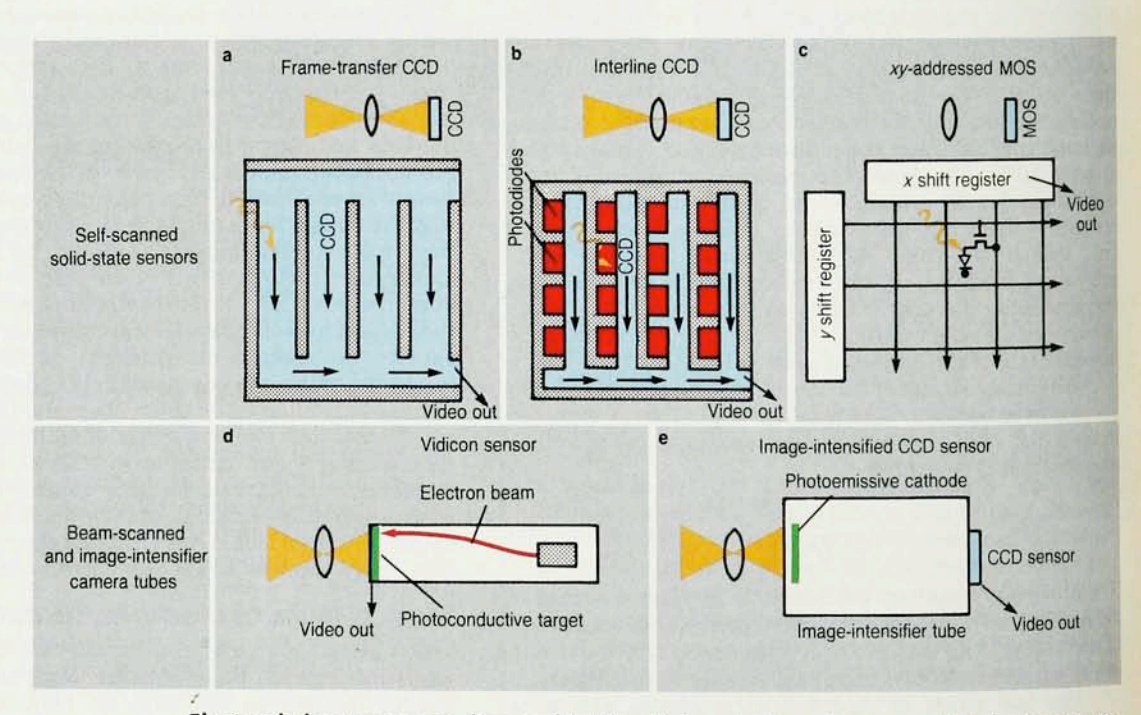
This sequential sampling does not degrade the sensitivity of the imaging system, provided the sensor can accumulate and measure the total photocharge released at each pixel during the entire exposure time between successive samplings. Each pixel must therefore have high dark resistance and charge storage capacitance. Conventional television cameras scan the entire image area 30 times per second in a raster pattern of about 500 horizontal lines.

Figure 4 illustrates five types of image sensors currently in use. Figures 4a and 4b are two layouts of two popular charge-coupled-device solid-state image sensors.5 The CCD is an analog shift register in which an entire sequence of charge packets can be shifted simultaneously along the surface of a silicon chip by applying clock voltages to overlying insulated gate electrodes. electric charge varies from one packet to the next. The sequence of charge packets is scanned as they move past an output electrode connected to an on-chip amplifier. In the "frame transfer" scientific sensor shown in figure 4a, the CCD registers are illuminated directly by the light from the imaged scene. In the "interline" camcorder sensor of figure 4b, the CCD registers are shielded from light; they perform line-by-line readout of the illuminated photodiodes interleaved between the CCDs. Figure 4c illustrates a so-called MOS (metal-oxide-semiconductor) solid-state sensor scanned by xy address strips connected to digital shift registers on the periphery. Figure 4d shows a cross section of a photoconductive vidicon camera-tube sensor scanned by an electron beam. Figure 4e is an imageintensified CCD sensor.

Among the fundamental factors determining the performance of an electronic imaging sensor are its resolution, the quantum efficiency of its photoreceptors and the signal-to-noise ratio of its output signal. Our discussion will be limited to these most basic performance criteria. We will compare the performance of several modern experimental sensors with the photon-counting ability of an ideal image sensor, and finally we will touch on the pickup of color signals.

Quantum efficiency of electronic sensors

The first requirement for a sensitive electronic sensor is that its photoreceptors provide an efficient conversion of radiant flux into electric current. The responsivities of several types of modern image sensors are plotted in figure 5, in mA/watt as a function of the wavelength of the radiant flux. The gray curves are lines of constant quantum efficiency, expressed as the ratio of output electrons to input photons. The quantum efficiency of the interline CCD (green) is lowered, relative to that of the frame-transfer CCD (red), by the reduced fraction of each pixel that can respond to light. The yellow curve applies to a nonstructured photoconductive layer of the kind used in vidicon sensors. Its quantum efficiency is higher than that of photoemitters (black curve) used in image intensifi-



Electronic image sensors discussed in this article. **a,b:** Two charge-coupled-device sensors. The third of the self-scanned solid-state devices (**c**) is a metal—oxide—semiconductor sensor scanned by *xy* address strips connected to shift registers. **d:** Beam-scanned photoconductive vidicon camera. **e:** Image-intensified CCD sensor. **Figure 4**

Responsivities of various sensors vs incident wavelength. The red curve is for a thinned, rear-illuminated frame-transfer CCD; the green curve, a front-illuminated interline CCD; the vellow curve, a continuous SeAsTe Saticon (vidicon) photoconductor; the black curve, an S-20 photoemitter used in intensifiers and early camera tubes. The gray contours are lines of constant quantum efficiency, labeled as the percentage of output electrons per input photon. Figure 5

ers and some camera tubes. Quite generally, photoemitters have a lower quantum efficiency than do solid-state sensors, but they permit the use of low-noise techniques for intensifying the resulting electron image to produce very sensitive sensors for detecting moving objects at night.

Long exposures to faint objects are limited by the accumulation of dark current. By cooling a silicon CCD sensor to reduce its dark current, one can increase its exposure time to more than a thousand seconds for recording very dim astronomical images.6 We will concern ourselves primarily with the performance of sensors that can observe moving scenes in real time, rather than with long time exposures.

Signal-to-noise

An ideal sensor operating with inadequate illumination will produce a television picture of degraded contrast, with brightness fluctuating at each point. Its electrical output will have a low signal-to-noise ratio, the noise in this case being the statistical fluctuation in the total number of photons incident on a pixel. A nonideal sensor will generate additional random noise, and additional "fixedpattern noise" if its image area contains structural nonuniformities. The fixed-pattern noise is most conspicuous at high signal levels; we will ignore it in this discussion.

Figure 6 illustrates a useful way of representing the video signal and its associated random noise. We plot $N_{\rm s}$, the total number of electrons accumulated at each pixel, against $N_{\rm p}$, the number of photons incident on that pixel during the exposure period. We assume an ideal sensor with a quantum efficiency η of 100%. The root-meansquare fluctuation of the signal N_s , called the "shot noise," is simply $N_{\rm s}^{1/2}$. Thus the signal-to-noise ratio also equals $N_{\rm s}^{1/2}$. If η is less than 100%, $N_{\rm s}$ is given by $\eta N_{\rm p}$ and the photoelectric shot noise is $(\eta N_{\rm p})^{1/2}$.

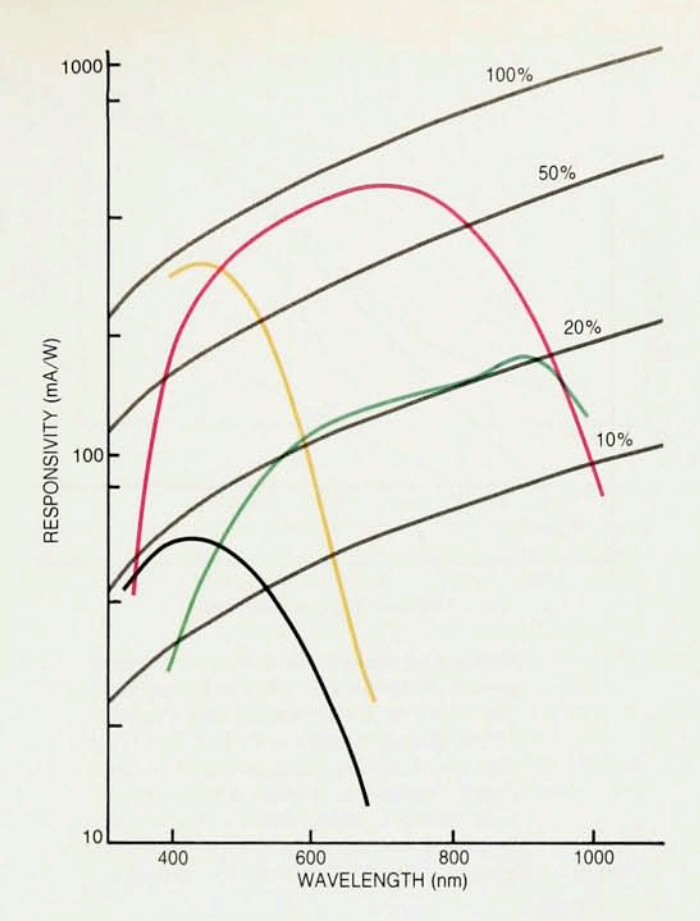
The additional random noise N_n generated by a nonideal sensor is shown in figure 6 by the horizontal line. The quantity N_n can also be expressed as an rms number of electrons per pixel, even when most of this noise is contributed by the first stage of the signal amplifier connected to the sensor.

To calculate the signal-to-noise ratio S/N of the output of a nonideal sensor, one sums the photoelectric shot noise and the noise generated by the sensor itself in quadrature. Thus

$$S/N = \frac{\eta N_{\rm p}}{\sqrt{\eta N_{\rm p} + N_{\rm p}^2}} \tag{2}$$

This equation will serve for comparing the performance of various solid-state and beam-scanned sensors with that of an ideal sensor.

In modern CCD sensors, the sensor noise N_n may include various components: reset noise and 1/f noise associated with the built-in output amplifier, fluctuations in the thermally generated dark current, and transfer noise when the transfer efficiency is poor. (Typical good

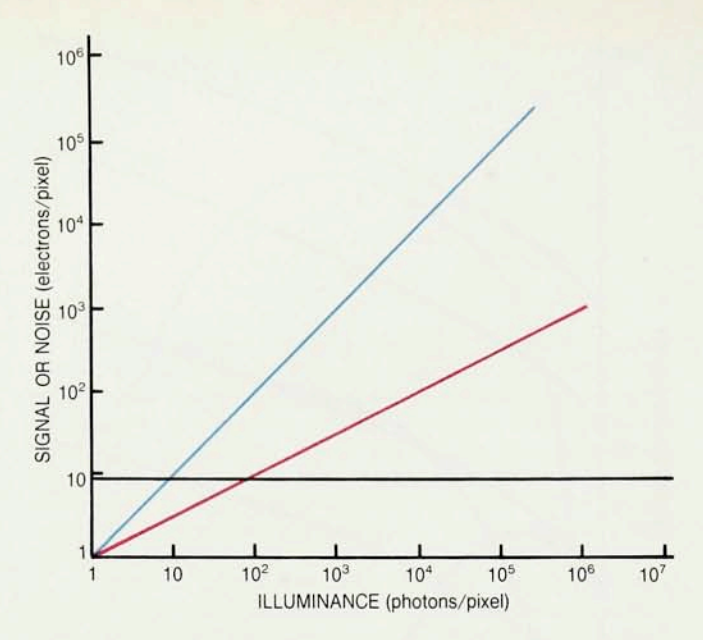


CCDs have transfer efficiencies exceeding 0.99999 per transfer.) The reset noise can be removed by external circuits, and dark-current noise is suppressed by cooling. Solid-state sensors of the xy-addressed MOS type lack the low-noise advantage of the CCD on-chip amplifiers, but their sensitivity for camcorder applications is comparable.

The sensor noise N_n in camera tubes depends on the method of generating the output. In the vidicon,7 the large capacitance of the photoconductive target's output electrode raises the noise level of the amplifier. In the old image orthicon tubes one obtained higher sensitivity by using a low-noise electron multiplier to raise the signal level in the modulated beam (returning from the storage target) well above the amplifier noise.8 But then the sensitivity was limited by the shot noise in the electron beam. The beam noise was substantially reduced in a later tube called the image isocon,9 by deriving the signal from only that fraction of the return beam scattered by the signal charge on the target. This modification in the electron optics reverses the polarity of the output signal and increases its fractional modulation.

For applications requiring operation at light levels so low that performance is limited only by photon noise, the best results are obtained by intensification of the electron image before it is stored.10 Such high-gain image intensification requires a photoemissive tube sensor incorporating intensifiers for the electron image. One can use a multiple-channel electron multiplier, an internal lightemissive phosphor or bombardment-induced conductivity in an internal storage target. One approach now being widely developed is to couple a light-emissive intensifier tube to an externally mounted CCD by fiberoptics.11 A more exciting approach, which might eventually lead to a non-vacuum intensified CCD, is avalanche multiplication in a vidicon-type photoconductive target. 12

For still lower light levels, where one wants to record and count the arrival of individual photons for an



Signal and noise of an electronic imaging sensor plotted against photon illumination. The signal (blue line) shown here implies 100% quantum efficiency. The shot noise (red line) is simply the square root of the signal. Additional random noise is shown here (black) as independent of the signal. Summing the two noise sources in quadrature gives the total rms noise level. **Figure 6**

unlimited period, one can record the accumulating image in an external digital memory from a nonscanning, position-sensitive silicon sensor.¹³ Such a photon-by-photon accumulation of an image can provide a striking demonstration of the wave-particle duality of the photon.

Resolution

The sharpness of an electronic image depends on the number of pixels into which the image is divided. For a beam-scanned camera tube, the effective number of pixels is twice the video bandwidth multiplied by the "useful" frame time: $\frac{1}{30}$ second minus the time used for horizontal and vertical blanking. The 525-line US television system, with its 4-MHz video bandwidth, thus has the equivalent of about 210 000 pixels. For high-definition television systems, Japan has proposed increasing the number of scan lines to 1125 and the luminance bandwidth to 20 MHz, a fivefold increase in the number of effective pixels.

At very low light levels, the limiting resolution is degraded by the decrease in signal-to-noise ratio. In accordance with equation 1, when S/N falls below the minimum level k necessary for recognition of individual pixels, the eye of the television viewer begins to integrate the signal from adjacent pixels, thereby increasing the effective pixel size. The resulting drop in resolution occurs whether the noise is photon shot noise or noise generated in the scanning process.

At high light levels (when S/N exceeds k), other factors limiting the resolution come into play. Figure 7 compares the measured response of a beam-scanned Saticon¹⁴ camera tube (black curve) and an interline CCD sensor¹⁵ (colored curves) to test patterns of straight lines. The response curves are plotted as functions of the number of television lines in the test pattern. For the CCD sensor, the response curves shown for the various vertical and horizontal modes are in fact its "modulation-transfer

functions," because they were measured with sinusoidal variation of line density across the test pattern.

Both of these experimental sensors were built several years ago for possible use in a high-definition television system. The improved response in the Saticon tube was obtained by reducing the size of the scanning beam. The CCD sensor incorporated more pixels (1280 horizontal by 970 vertical) than is usual for a television-type CCD. Its sensitivity was 0.06 A/watt at a wavelength of 550 nm, corresponding to a quantum efficiency of only 14%. More recently, interline CCD sensors with still higher definition and much higher quantum efficiency have been reported. 16

The fact that only a fraction of each pixel area in most self-scanned sensors is photosensitive has important consequences for their resolution as well as their quantum efficiency. The geometric limitation on the modulation-transfer function for a solid-state sensor is given by the Fourier transform of its photoresponsive area. For a responsive area of length Δx separated in the x direction from its neighbor by a repeat distance of d, the geometric modulation-transfer function in the x direction is d

$$MTF_{geom} = \frac{\sin\left(\frac{\pi}{2} \frac{f}{f_{N}} \frac{\Delta x}{d}\right)}{\frac{\pi}{2} \frac{f}{f_{N}} \frac{\Delta x}{d}}$$
(3)

where f is the spatial frequency of the sine-wave test image and $f_N = 1/2d$ is the Nyquist frequency, the maximum spatial frequency that can be reconstructed by this configuration.

For the experimental interline CCD sensor of figure 7, the Nyquist frequency is 960 television lines in both the horizontal and vertical directions. The high MTF response observed in the horizontal direction (red curve) at the Nyquist frequency is predicted by equation 3, if we take Δx to equal d/2. The lower response observed in the vertical direction (blue) for the frame-integration mode is what one expects for $\Delta y = d$. In the field-integration mode, where all rows are sampled in pairs so that $\Delta y = 2d$ (green curve), the response vanishes at the Nyquist frequency. If any spatial frequencies in the scene exceed $f_{\rm N}$, they will appear as false frequencies because of a process called "aliasing," caused by the overlap of spectra from adjacent pixels. Attempts to reduce aliasing by optically prefiltering the image to remove spatial frequencies above the Nyquist limit have resulted in a serious reduction of response. In spite of the aliasing problem, interline CCDs are widely used today in camcorders.

Another factor that can degrade MTF response in frame-transfer CCDs occurs when carriers excited on the back of the thinned silicon chips spread to adjacent

pixels by diffusion. The MTF can also be reduced by poor transfer efficiency in the CCD registers, but advances in fabrication technology have greatly alleviated this problem.

Thin-film photoconductors of the kind used in vidicons are capable of very high resolution because no structure is required between pixels. These amorphous or polycrystalline photoconductive layers also suffer much less lateral diffusion of charge than does single-crystal silicon. Depositing such photoconductors on top of interline CCD scanners yields much improved quantum efficiency, because the photoconductor need not be interrupted by the CCD registers. A high-definition television sensor of this type having two million pixels overlaid with amorphous silicon photoconductor has yielded a quantum efficiency of 60-70% over the entire visible wavelength range. 16 The sensitivity of this sensor is shown by curve C of figure 8, which compares various modern sensors.

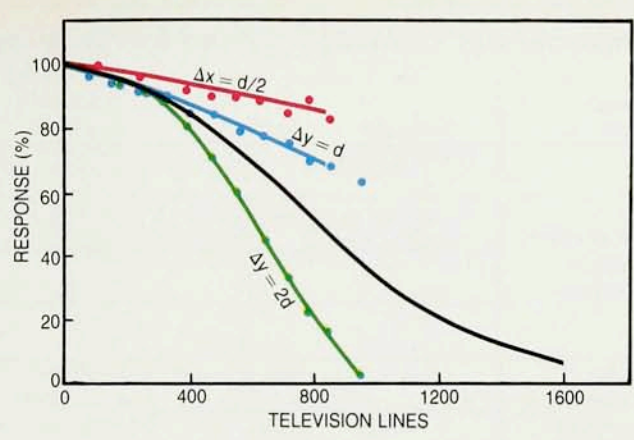
Performance comparisons of modern sensors

It is interesting to examine how closely modern electronic sensors approach the performance limitations set by the number of photons in the optical image. The table on page 32 summarizes the published characteristics of the developmental sensors we have discussed here. Figure 8 shows the calculated signal-to-noise ratio curve for each of these devices, plotted as a function of N_p , the number of incident photons per pixel. Equation 2 was used to derive S/N from the measured values of quantum efficiency η and the sensor noise N_n . Such a plot is useful for comparing the photon-counting performance of sensors of assorted sizes and numbers of pixels with an ideal sensor (red curve) that generates no additional noise and has 100% quantum efficiency. The leveling off of S/N at high exposure in some of these curves indicates the point at which the photocharge completely fills the pixel's storage capacitance.

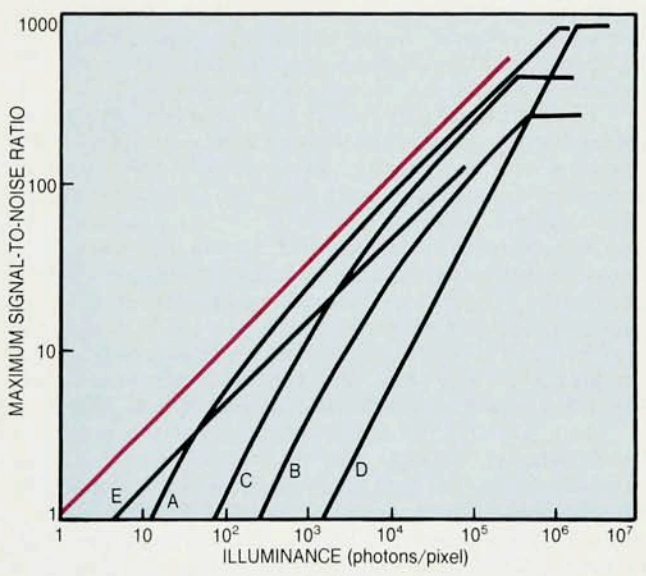
The superior performance of the large scientific CCD shown by curve A was achieved with $\eta=70\%$ and $N_{\scriptscriptstyle \rm n}=9$ electrons (rms). It should be noted that these values were improved by slow scan readout at a data rate of only 5×10^4 pixels/sec, with the sensor cooled to -90 °C. The other sensors were designed for television operation with concurrent exposure and readout, and with added "antiblooming" structures built into the CCDs for control of excess illumination. The noise measurements on these other sensors were made with wide bandwidth and without cooling.

Color pickup with a single sensor

Modern color television systems are based on the encoding of three simultaneous video signals corresponding to the red, green and blue components of the image. The earliest



Sine-wave (MTF) responses of an experimental interline CCD15 (colored curves) compared with the square-wave response of an experimental Saticon camera tube14 (black curve), plotted against the number of television scan lines. The horizontal CCD response curve (red) shows that $\Delta x = d/2$ in equation 3. The vertical response curve for the frame-integration modes (blue) shows that $\Delta y = d$. In the field-integration mode, the vertical response of the CCD (green) vanishes at the Nyquist frequency (960 television lines) because $\Delta y = 2d$. Figure 7



Photon-limited signal-to-noise ratio vs incident light for various sensors, from equation 2. (See table on page 32 for details.) The red curve represents an ideal sensor with perfect quantum efficiency and no noise other than photon shot noise. Curve A is for a cooled frame-transfer CCD with slow readout. B is for a high-definition interline CCD. C is also for a high-definition interline CCD, but with an overlying photoconductive layer. D describes both an xy-addressed MOS color sensor and a beam-scanned silicon vidicon. The latter has the higher sensor noise of the two, but its quantum efficiency is also much higher. E describes intensifier tubes with enough gain to override sensor noise. Their quantum efficiency is typically 20%. Figure 8

Characteristics of modern electronic image sensors

Sensor type	Example	Application	Number of pixels	Image area (mm²)	Sensor noise N _n (electrons/pixel)	Quantum efficiency η	Performance (figure 8)
Self-scanned silicon sensors	Frame-transfer CCD	Astronomy	2024× 2024	55×55	9 (slow scan)	70% (thinned)	Curve A (ref. 6)
	Interline CCD	High-definition TV	1280× 980	12.7× 9.5	36	14%	Curve B (ref. 15)
	Photoconductor over CCD	High-definition TV	1920× 1036	14.0× 7.8	52	65%	Curve C (ref. 16)
	MOS xy-address	Color camcorder	649× 491	8.6×6.5	745	40%	Curve D (ref. 18)
Photo- conductive camera tubes	Saticon	High-definition TV	1 050 000 (at 20 MHz) 210 000 (at 4 MHz)	12.7× 9.5			(ref. 14)
	Si vidicon	Low light levels			1500	90%	Curve D
Image intensifiers for ultra- low light	Image- intensified CCD	Scientific	684×576 (CCD array)	18 mm (diagonal)	High gain overrides	20%	Curve E (ref. 11)
	Photon- counting imager	Astronomy	512×512 digital store	Position- sensitive detector	sensor noise	20%	(ref. 13)

color cameras used a three-way dichroic image splitter with three conventional camera tubes to generate the three signals. In spite of their complexity and registration problems, the three-tube cameras give excellent pictures; they are used principally for studio broadcasting and high-definition television. Color cameras using three CCDs are much more compact, and they are beginning to match the three-tube cameras in picture quality. Camcorders for home use employ single-sensor cameras with a special vidicon or a self-scanned solid-state sensor.

In the modern approach to tricolor sensors, a striped or checkerboard pattern of three or more color filters is superposed over the image plane of the sensor—a scheme somewhat analogous to early color photography systems. This approach poses the electronic problem of identifying and separating the three signal components. For camera tubes, in which the precise location of the beam is not accurately known, two methods have been used. One requires adding an electrode structure to the photoconductive target. The other method requires orienting the filter stripes in such a way that the color signal can be identified by virtue of its resulting frequency or phase.

In a self-scanned sensor, color signal separation is much simpler, because the location of each pixel is precisely known in time and space. When a checkered filter pattern of three or more colors is located in registry with the pixel array of a CCD or MOS sensor, the color components can be derived from one or more outputs. For example, an *xy*-addressed MOS sensor used in a color camcorder provides green, cyan, white and yellow output signals, each to a separate lead. ¹⁸ The colors and pattern arrangements must be chosen to minimize spurious color aliasing. No one has as yet reported the development of a nonstructured color sensor analogous to layered color film.

As long as the principal task of electronic sensing remains simply the viewing of optical images, the serially scanned sensors we have discussed will be competent electronic eyes for most purposes. However, sensors are increasingly being used in conjunction with computers for complex tasks such as pattern recognition. For such tasks a parallel system might be better than a sequentially scanned system. Experimental "smart" sensors have been built, patterned after the biological structures of the retina 19 and incorporating multiple-level integrated circuits. Oceanly, the future development of image sensors will have much in common with neural computing.

References

- 1. N. Ben-Yosef, A. Rose, J. Opt. Soc. Am. 68, 935 (1978).
- 2. J. L. Schnapf, D. A. Baylor, Sci. Am., April 1987, p. 40.
- A. Rose, Vision: Human and Electronic, Plenum, New York (1973).
- A. Rose, in Advances in Electronics, vol. 1, L. Marton, ed., Academic, New York (1948), p. 131.
- C. H. Séquin, M. F. Tompsett, Charge Transfer Devices (Advances in Electronics and Electron Physics, suppl. 8), L. Marton, ed., Academic, New York (1975).
- M. Blouke, B. Corrie, D. Heidtmann, F. H. Yang, M. Winzenread, M. L. Lust, H. H. Marsh IV, J. R. Janesick, Opt. Eng. 26, 837 (1987).
- P. K. Weimer, S. V. Forgue, R. R. Goodrich, Electronics 23, 70 (1950).
- 8. A. Rose, P. K. Weimer, H. B. Law, Proc. IRE 34, 424 (1946).
- 9. P. K. Weimer, RCA Rev. 10(3), 366 (1949).
- G A. Morton, J. Ruedy, Advances in Electronics and Electron Physics, vol. 12, L. Marton, ed., Academic, New York (1960), p. 183.
- L. K. Van Geest, in Photoelectronic Imaging Devices (Advances in Electronics and Electron Physics, vol. 74), B.L. Morgan, ed., Academic, New York (1988), p. 1.
- K. Tanioka, J. Yamazaki, K. Shifara, K. Taketoshi, T. Kawamura, S. Ishioka, Y. Takasaki, IEEE Electron Dev. Lett. EDL 8, 392 (1987).
- Y. Tsuchlya, E. Inuzuka, T. Kurono, M. Hosoda, J. Imaging Technol. 11(5), 215 (1985).
- Y. Isozaki, J. Kumada, S. Okude, C. Ogusu, N. Goto, IEEE Trans. Electron Dev. ED-28, 1500 (1981).
- I. Akiyama, T. Tanaka, E. Oda, T. Kamata, K. Masubuchi, K. Arai, Y. Ishihara, in *Digest of Technical Papers*, 1986 IEEE Int. Solid-State Circuits Conf., IEEE, New York (1986), p. 96.
- S. Manabe, Y. Matsunaga, M. Iesaka, S. Uya, A. Furukawa, K. Yana, H. Nozaki, Y. Enda, Y. Egawa, Y. Ide, M. Kimura, N. Harada, Digest of Technical Papers, 1988 IEEE Int. Technical Conf., IEEE, New York (1988), p. 50.
- D. F. Barbe, S. B. Campana, in Advances in Image Pickup and Display, vol. 3, B. Kazan, ed., Academic, New York (1977), p. 171.
- M. Noda, T. Imaide, T. Kinugasa, R. Nishimura, IEEE Trans. Consumer Electron. CE-32, 329 (1986).
- M. Sivilotti, M. A. Mahowald, C. A. Mead, in Stanford Confon Very Large Scale Integration, P. Losleben, ed., MIT P., Cambridge, Mass. (1987), p. 295.
- K. Kioi, S. Toyoyama, M. Koba, Technical Digest, 1988 IEEE Int. Electron Devices Mtg., IEEE, New York (1988), p. 66.